Composite Structures xxx (xxxx) xxx–xxx

Contents lists available at ScienceDirect

Composite Structures

journal homepage: www.elsevier.com/locate/compstruct

TLS-based composite structure deformation analysis validated with laser tracker

Xiangyang Xu[a], Johannes Bureick[a], Hao Yang[a,b,*], Ingo Neumann[a]

[a] Geodetic Institute, Faculty of Civil Engineering and Geodetic Science, Leibniz University Hanover, Germany
[b] Jiangsu University of Science and Technology, Zhenjiang City, Jiangsu Province, PR China

ARTICLE INFO

Keywords:
Composite arch
Deformation analysis
Data extraction
B-spline fit
Point clouds
Terrestrial laser scanning

ABSTRACT

This paper focuses on the adjustment of B-spline approximation to terrestrial laser scanning (TLS) data and its contribution to deformation analysis of composite arched structures. The deformation of an arch structure under static loading conditions are investigated with TLS technology which is accurate, time-efficient, and capable to obtain dense 3D coordinates of point clouds for the measured objects.

Highly accurate approximation methods for the point clouds data are extremely important for structural deformation analysis. The innovation of this paper is that parameters of B-spline is optimized with laser tracker (LT) to improve the accuracy of deformation monitoring and analysis, where the result is justified with LT data and the uncertainties are analyzed. It is revealed that optimized B-spline approximation agrees better with LT result. The improvement to the B-spline curve with minimum standard deviation reaches 52%, and its improvement to polynomial approximation reaches 77%.

1. Introduction

Nowadays, with the increasingly complex architectures, one of the key problems in civil engineering is the improvement of the reliability of the constructed structures. Deformation monitoring of the static and dynamic behavior of engineering structures is a hot topic which detects potential damages and avoid malfunction [1]. Three-dimensional (3D) terrestrial laser scanning (TLS) technology has better flexibility compared with the traditional monitoring methods in civil engineering, especially in the later period of engineering projects, due to no requirement of pre-embedded sensors in the structures. Many surveying methods, e.g. total stations and theodolites are also used in deformation monitoring but they are mostly point-wise surveying methods. The competence of TLS lies in the surface-based monitoring with the acquisition of high-density point cloud within a short time [2]. However, the research of TLS-based method for deformation monitoring is still developing. One of the issues that remains is to improve the accuracy during measurement and modeling for deformation analysis with TLS technology.

1.1. Terrestrial laser scanning

TLS is a geodetic technique for rapid acquisition of dense gridded 3D point cloud on object surface, which changes the traditional single-point data acquisition to an area-oriented mode. The main measuring principles are summarized as: time difference, phase difference and triangulation relationship during the emission, reflection and receiving of the laser beam [3]. A new technique for deformation monitoring is provided by TLS with the non-contact, high-speed acquisition of the original mapping data [4–9]. However, the raw point cloud data is discrete and scattered information, which contains a few errors and uncertainties. Thus, a method to reconstruct the continuous 3D model is required for the extracted point cloud. This paper optimized the sophisticated procedure for approximation of B-spline, and proposed that the higher accuracy of B-spline doesn't always leads to better deformation analysis, where the relation between the point clouds and the deformation behavior should be accounted. The mathematical approximation models are justified with LT data for a highly accurate deformation analysis of structures.

1.2. B-spline approximation

Free-form curves and surfaces, such as Bézier or B-splines, are suitable mathematical functions to approximate extracted point cloud. Especially B-splines meet the requirements of an exact but also smooth approximation of point cloud.

A curve point $\mathbf{C}(\bar{u})$, lying on a B-spline curve, is calculated by the totalised linear combinations of the basis functions $N_{i,p}(\bar{u})$ and the

* Corresponding author at: Geodetic Institute, Faculty of Civil Engineering and Geodetic Science, Leibniz University Hanover, Germany.
E-mail address: Yang@gih.uni-hannover.de (H. Yang).

https://doi.org/10.1016/j.compstruct.2017.10.015
Received 26 September 2017; Accepted 4 October 2017

control points $\mathbf{x}_i$ (see Eq. (1)). $n + 1$ linear combinations and the same amount of control points and basis functions contribute to the sum respectively to $\mathbf{C}(\bar{u})$. p is called the degree of the basis function. The so called location parameter $\bar{u}$ describes the position on the B-spline curve. Usually, the starting location parameter of the curve is defined with 0 and ending location parameter is defined with 1. The basis functions $N_{i,p}(\bar{u})$ were calculated using a recursive function introduced by [10] and [11] (see Eq. (2)–(4)).

$$\boldsymbol{C}(\bar{u}) = |x(\bar{u}),y(\bar{u}),z(\bar{u})| = \sum_{i=0}^{n} N_{i,p}(\bar{u})\boldsymbol{x}_i;\boldsymbol{x}_i = [x_i,y_i,z_i] \tag{1}$$

$$N_{i,0}(\bar{u}) = \begin{cases} 1 & if\ u_i \leqslant \bar{u} \leqslant u_{i+1} \\ 0 & otherwise \end{cases} \tag{2}$$

$$\mathrm{N_{i,p}}(\bar{u}) = \frac{\bar{u}-u_i}{u_{i+p}-u_i}\mathrm{N_{i,p-1}}(\bar{u})\frac{u_{i+p+1}-\bar{u}}{u_{i+p+1}-u_{i+1}}\mathrm{N_{i+1,p-1}}(\bar{u}) \tag{3}$$

$$\boldsymbol{U} = |u_0,\ldots,u_m|\ with\ u_i \leqslant u_{i+1}, \quad i \in \{0,\ldots,m-1\} \tag{4}$$

The so called knot vector $\mathbf{U}$ consists of $m + 1$ ($with\ m = n + p + 1$) knots, arranged in a non-decreasing order (Eq. (4)). During the approximation process with B-splines four important steps have to be accomplished: model selection, parameterisation of the data, determination of the knot vector and estimation of control points. The step "model selection" comprises the adequate choice of p and $n + 1$. In the step "parameterisation of the data" the location parameter $\bar{u}$ has to be determined for every data point. The step "determination of the knot vector" all $m + 1$ knots have to be determined. In the final step "estimation of control points", the $n + 1$ control points $\mathbf{x}_i$ were estimated, using a Gauss-Markov-Model.

For a more detailed description of the steps of the approximation process, the extension to B-spline surfaces and the relation between B-splines and other free-form curves and surfaces, see for example [12] or have a look in standard literature like [13,14]. [15] applied B-spline method to investigate cross-section determination based on laser scanning data.

1.3. Deformation and change detection

The purpose of deformation monitoring is to detect quantitatively the change of geometric state of a scene or object [16]. In many engineering fields, e.g. composite structures, detection of structural micro deformation or change was studied with X-ray, ultrasonic wave, IR thermography etc. [17–20]. Remote sensing, GPS and image processing also gained attention in deformation monitoring [21–23]. Traditional deformation monitoring with TLS focuses on registration and point-based deformation monitoring [2]. However, the systematic error of laser scanner and environmental factors usually arouse the uncertainties to single point. Furthermore, because the accuracy of local point clouds are variously influenced by the measurement geometry and surface properties, it is challenging to decide globally if the object is locally changed [7]. Object- or morphology-oriented analysis with TLS is a new direction for deformation analysis [2]. However, the influence of factors and significance of accuracy of free-form 3D modeling for the point cloud is not reported in detail.

2. Experimental setup

An experiment was designed to monitor the deformation of an arch structure, whose geometric size is about 2 m of span, 10 cm of thickness and 1 m of width. The experiment was carried out to investigate highly accurate B-spline curve in the analysis of deformation behavior of arch structure with TLS measurement. In this paper, the arc-shaped part of the object is the focus for structural monitoring, because it bears the main load and shows significant deformation. The arch was supported by two platforms, where the left one is stable but the right one is horizontally movable. Thirteen epochs data are collected, where in every epoch load was applied with speed 33 N/s for 20 min and then paused about 10 min for measurements.

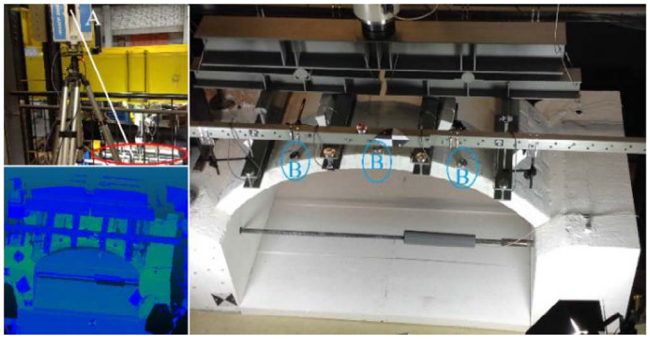

Fig. 1. Experiment setup.

As shown in Fig. 1A, a fixed standpoint of TLS is set on the second floor. The scanning direction is drawn with white line and the scanning area is presented with red circle, where scanning distance is approximately 6 m and the average point density is 20 points/cm^2. The TLS used here is Z + F Imager 5006, which is a phase-based-principle instrument.

The right figure in Fig. 1 is a detailed picture of the experiment. The jack located in the middle position of the arch and then the load was distributed to four evenly-distributed positions through steel beams and bearings. Three corner cube reflectors (CCR) measured by the laser tracker were set on the top surface of the arch (B in Fig. 1). However, the arc-shaped object is occluded with objects, e.g. steel I-beams. A sketch of the specimen monitored which is colorized with reflectivity values using Z + F Laser Control software is depicted in the lower left in Fig. 1. The green parts show the arch structure and two supports and the blue parts are surroundings, which needs to be separated for more accurate analysis.

3. Data analysis

In this paper, the scanned raw point cloud is processed where the boundary in the frontal side surface is extracted and approximated by means of high-accuracy B-spline curve with MATLAB. Deformation in 3D is calculated based on the curves fitting.

3.1. Point cloud extraction

Point cloud extraction is performed to separate the area or curve which is of main interest for deformation analysis. In this experiment, the boundary in the frontal side surface reflects the key deformation in the vertical direction, and it can be observed by laser tracker. Thus, the point cloud of side boundary has to be extracted. The task is carried out with two steps, the first is the extraction of the side surface and the second is the extraction of the side boundary curve.

The workflow of point cloud extraction is presented in Fig. 2. Firstly, the point cloud is preliminarily processed to keep only the area of interest, which can reduce the unnecessary computation of the remaining parts. Secondly, the density of the point clouds is computed and analyzed with window-neighborhood method. Thirdly, threshold is determined based on the density information. Thereafter, the point cloud is filtered and extracted. The filtered point cloud goes through a cycle quality checking in the case of boundary extraction. The threshold is justified to improve the extraction in terms of blank and noise, because the extraction is sensitive to the threshold value. If the point cloud is not qualified, the threshold is modified and a new filtering will be carried out, on the contrary, if the point cloud is qualified, it will be output for further processing.

The TLS scanner obtained the main details of the top and frontal

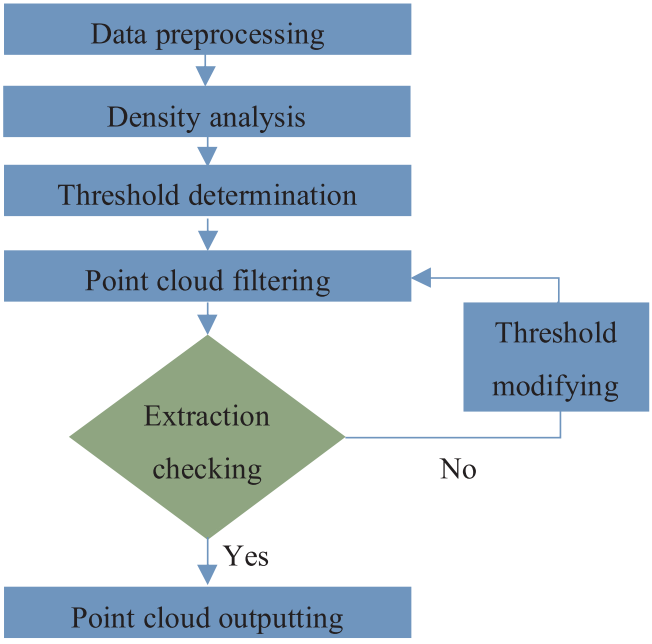

Fig. 2. Work flow of point cloud extraction.

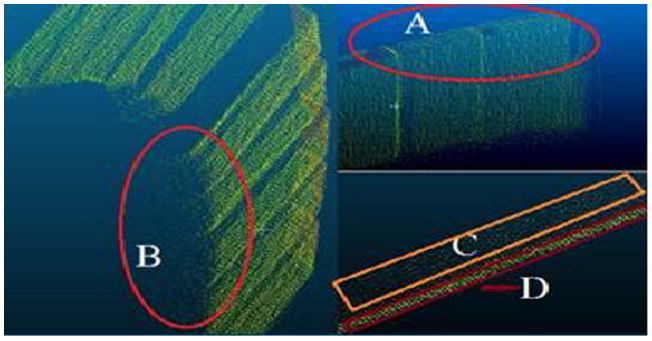

Fig. 3. Point cloud details of the arch area.

side surfaces of the arch, while the lower and rear surfaces are occluded. The intersection of the top surface and the frontal side surfaces is a curve, which undulates according to the combination structures of bricks and binders (see Fig. 3A). There are some error points in the lower boundary of the side surface which are not contained in the side surface (see Fig. 3B), however, they are visually obvious and separable through density difference.

The point cloud of the side surface is found in the top view, i.e. X-Y plane, which is D in Fig. 3, by a clear dense difference to C in Fig. 3 which should be the point cloud of top surface. Point cloud D is denser than C. The main reason is that: TLS scanned the surface and obtained the outermost point cloud and the point cloud D are stacking in thickness direction from the top view. As the calculation shows, the thickness of the arch is 10 cm, the laser point step in vertical direction is about 0.2 mm, which means the points D in the top view represents point cloud in the number of several tenfold times of visual density. However, the point density on the top surface is similar with scanning density. An extraction method is carried out to separate the side surface and the boundary curve in the following by means of density recognition and data filtering.

At first, the density is quantified within a square window of 1*1 cm for each point, which means that a point with coordinates value Px, Py and Pz, defines a square window enclosed by $Px - 0.5$, $Px + 0.5$, $Pz - 0.5$ and $Pz + 0.5$ in X-Z plane. The number of points in this window is recorded as quantified density (QD). Since the density in the side surface is significantly larger, the threshold of the QD for the side surface which differs with other points is determined to filter the data. The percentage of different QD is presented in Fig. 4a, where the distribution corresponding with side surface is marked with red circle. The bars in the demarcation position have significant increase to the excluded area, as marked in red points in Fig. 4a. The threshold of the filter for the side surface is defined as 840 as the red point (see Fig. 4a).

The side surface is analyzed thereafter in X-Z plane to extract the boundary curve. The side surface has a relatively uniform distribution in X-Z plane, therefore, the QD is changing gradually for the middle parts of the surface. And it should be larger than the boundary and occlusion area. The distribution of the neighbor number of the extracted side surface can be seen from Fig. 4b, where the peak of the QD (QD_p) marked with red point in the Figure is 136.

Statistically, the points in the boundary area have on average half neighbors of the center area (QD_c), which is set initially as $QD_p/2 = 68$. Since more data points result theoretically in a higher accurate curve fitting, the threshold range is set as $[68 - t, 68 + t]$ $(t = 30)$ previously. The range was carefully tested, where the variables QD_c and t are increased/decreased by 5 each time, and the figure of extraction was drawn and checked. It reveals that higher threshold value will include noisy points while a lower one will exclude some valid points and generate blank.

The extraction data is virtually validated with two requirements, the first is that there is no noise from the middle of the surface, and the second is that the boundary curves are extracted as complete as possible. The extraction will also be validated through the final curve fitting accuracy, since the curve is fitted only with the extracted point cloud.

3.2. Curve fitting

The extracted point cloud is approximated by a B-spline curve. The

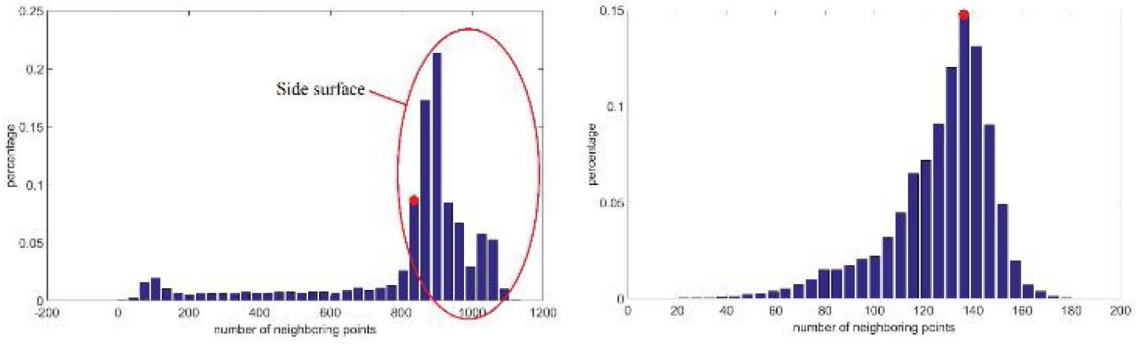

a) Neighbor number b) neighbor points in side surface

Fig. 4. Distribution of neighbor number.

mathematical basics are described in Section 1.2. In the step "model selection" the parameters p and n + 1 were set as two situations to figure out higher accuracy solution of the approximations, one is curve Ba with more control points (p = 2, n + 1 = 100), and the other is Bb with higher order (p = 3, n + 1 = 21). For both curves Ba and Bb, the "parameterization of the data" is realized by the chord length method [14]. The "determination of the knot vector" is accomplished in each case using the average-method of Piegl and Tiller [14]. For this step it is possible to use more sophisticated methods [24] to determine the knot vector, but due to the rather simple shape of the point cloud and the rather high number of parameters these methods do not yield significantly better results. In the final step the control points are estimated using a Gauss Markov Model [14] in each case.

In addition to that, a 2D polynomial curve is applied to verify the accuracy of the approximation in vertical direction. Polynomial curve was successfully applied in many cases [25]. Generally, the degree of the polynomial curve is the key parameter in the estimation. Model testing was carried out for the selection of a best-fit order for the polynomial curve. The accuracy of the approximated curve is calculated with standard deviation (SD) of the residuals between the curve and the raw point cloud. A smaller value means a better approximation to the raw point cloud.

3.3. Deformation calculation

Deformation of the boundary curve is represented by the distance between fitted curves, after the curve is approximated according to the data from different epochs.

Deformation of surface varies in definition of direction, including normal distance, minimal distance, vertical distance, etc. First of all, the three epochs are depicted as three functional curves. The first curve, related to epoch 0, is discretized to a very dense point cloud with e.g. 10,000 points. The second and third curve, related to epoch 1 and 2, are discretized at the positions of the adjusted observations in each case. So the number of points in these point cloud conforms to the number of scanned points. For each discretized point in epoch 1 and 2 the minimal distance to the dense point cloud of epoch 0 is calculated. The deformation of epochs 1 and 2 with respect to epoch 0 are presented in Fig. 5.

All curves were approximated with Ba. It can be observed that the deformation is within 10 mm for both epochs and that the larger deformation deviates the center position of the curve. Deformation of the boundary curve is represented by the distance between fitted curves, after the curve is fitted according to the data from different epochs.

4. Result

The paper emphasizes the significance of high-accuracy curve model based on TLS measurement for deformation analysis of the arch structure. In many engineering cases, polynomial model is also widely adopted. In order to find out how much accuracy would be increased in the case study, two B-spline curves and a polynomial curve for epochs 1 and 2 are compared to investigate the accuracy of fittings for deformation analysis.

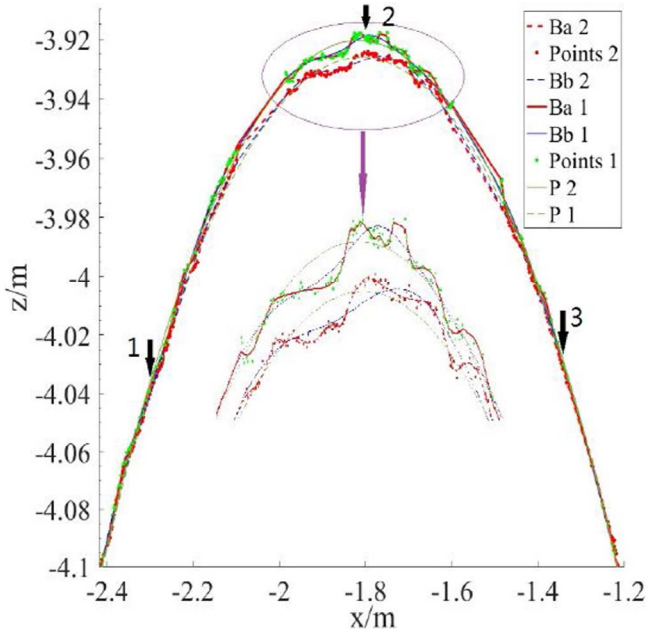

Fig. 6. The performance of different fitted curves.

The result is presented in Fig. 6, where Ba is B-spline curve with degree p = 2 and number of control points n + 1 = 100, Bb is B-spline curve with degree p = 3 and number of control points n + 1 = 21, P is polynomial curve whose number of parameters is 21, similar to Bb. The positions of CCRs are marked with black arrows. It is observed in Fig. 6 that Ba describes the local characteristics of the point cloud better than Bb, and P is not competent in following local shapes.

The standard deviation of Ba, Bb and P in Z-axis direction for epochs 1 and 2 (E1 and E2) are shown in Table 1, where SD means standard deviation. Table 1 shows that Ba is as expected the best fitting to the point cloud because its standard deviation is smallest in both epochs.

The fitness of Ba to the raw point cloud is proved by the quality of raw point cloud data, which is obtained from the intensity values of the point cloud [26]. The uncertainties of approximated point cloud falls mainly in 0.7–0.8 mm, with an agreement to the standard deviation of Ba. It is proved that the error of Ba is balanced with that of raw point cloud and the curve Ba fits best to the raw point cloud.

The maximum deformation in z axis direction is shown in Table 2, which is 5.6 mm for epoch 1 and 9.76 mm for epoch 2. The positions of the maximum deformation are recorded.

The deformation of the top surface is acquired with surface approximation for the arch structure, which verifies the result of the curve description. The surface shown in Fig. 7 is the top view of the spatial deformation of the top surface of epoch 2, where the blue point is the position of the spatial maximum deformation. It is observed that the deformation is asymmetric and the main deformation shift to the left of the exact middle position, which verifies the conclusion from curve fitting in Fig. 6.

Laser tracker is applied in this experiment for external verification

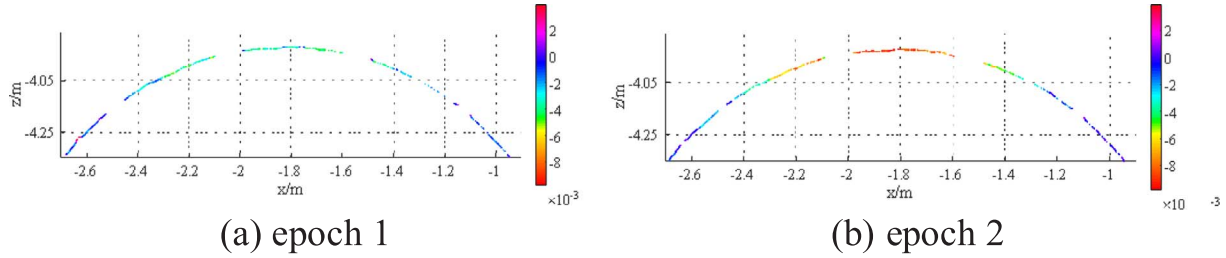

Fig. 5. Deformation distribution of epochs 1 and 2.

Table 1
Standard deviation of different curves.

SD in Z-axis (mm)	Ba	Bb	P
E1	0.80	1.45	2.40
E2	0.70	1.40	2.10

Table 2
Maximum difference in z-axis direction.

Data set	Max dz (mm)	Position (m)
E1–E0	5.60	x = −2.11 y = 3.42 z = −3.96
E2–E0	9.76	x = −1.92 y = 3.51 z = −3.93

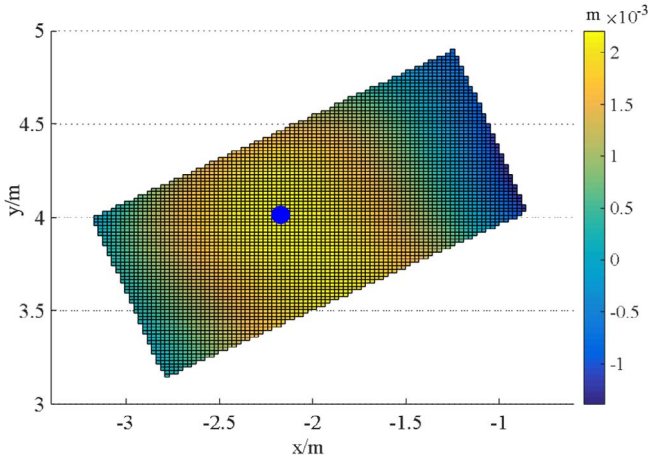

Fig. 7. Position of maximum displacement on top surface.

Table 3
Residuals between CCR and the points on fitted curves.

		Epoch 1 (mm)	Epoch 2 (mm)
Ba	CCR1	−3.91	−2.66
	CCR2	−1.54	−1.61
	CCR3	−1.95	−1.30
Bb	CCR1	−3.61	−2.35
	CCR2	+0.67	−0.77
	CCR3	−1.95	−0.16
P	CCR1	−3.87	−3.53
	CCR2	−3.78	−3.41
	CCR3	−3.84	−3.60

of the deformation results. Three CCR were set near the boundary on the top surface. The x, y and z coordinates of the three CCR are obtained with 0.1 mm (SD) accuracy during each epoch. Because CCR are not exactly on the boundary curve, the closest points to three CCR on the fitted curves are searched and the displacement of the searched points are analyzed. Table 3 shows residuals between CCR and corresponding points on fitted curves, where Bb leads to the smallest differences with LT result. Its improvement to Ba reaches 52%, to P reaches 77%, which is marked in bold.

It is demonstrated in Table 3 that the Bb with less control points leads to a deformation result closer to external CCR. The indicator occurs for all three CCR and for both two epochs. Apparently, it is proved in Table 2 that the curve Ba fits best to the raw point cloud. A possible origin for the interesting distinctive is that the point cloud contain noise and the Ba restores the shape of point cloud but it also inherits the noises contained. On the contrary, P curve is smooth enough to eliminate the noise, but it also removes the detailed local characteristics of the point cloud.

5. Conclusion

The B-spline approximation is adopted to construct highly accurate 3D curve, where the parameters of B-spline are compared. The B-spline fittings Ba and Bb are analyzed with 99 and 19 control points respectively, where the fitness to the raw point cloud is judged by the standard deviation of the curve. It shows that standard deviation of Ba is the smallest and agrees with the uncertainties of point cloud. It proved that the point cloud extraction has few influence on the final curve fitting. The deformation analysis are carried out using the closest distance. The maximum deformation and its position agree with surface approximation of the top surface of the arch. Possible error sources of the deformation analysis could be LT, laser scanning process, edge extraction and 3D approximation. The error of LT is generally 0.1 mm, which can be neglected; the error from point cloud data brought by laser scanning process and edge extraction is similar with the error of 3D approximation result, which is 0.7–0.8 mm.

The laser tracker externally verified the value of the deformation through CCR. Only three CCRs are adopted in this paper as a test, however, more CCRs will increase the reliability of the verification. The Bb with less control points leads to a deformation result closer to all external CCRs for both two epochs. It indicates that the point cloud contain noise and the Ba restores the shape of point cloud but it also inherit the noises contained. On the contrary, P curve is smooth enough to eliminate the noise, but it also removes the detailed local characteristics of the point cloud.

To conclusion, B-spline is a suitable method to adopt in deformation analysis, because of the capability to reflect the local characters, but it doesn't mean B-spline with higher accuracy can lead to higher accuracy deformation analysis, due to it also inherits the noises contained. External tools of laser tracker can be adopted to validate the deformation results. It is feasible for the next step to calibrate the number of control points and degree of B-spline curves based on the validation.

Acknowledgments

The publication of this article was funded by the Open Access Fund of the Leibniz Universität Hannover. The authors gratefully acknowledge the support of Massivbau Institute to this research work and also would like to acknowledge the support of Natural Science Foundation of Jiangsu Province (No: BK20160558).

References

[1] Gumus K, Erkaya H, Soycan M. Investigation of repeatability of digital surface models obtained from point clouds in a concrete arch dam for monitoring of deformations. Boletim Geodesicas de Ciencias 2013;19:268–86.
[2] Mukupa W, Roberts GW, Hancock CM, Al-Manasir K. A review of the use of terrestrial laser scanning application for change detection and deformation monitoring of structures. Survey Rev 2017;49:99–116.
[3] Vosselman G, Maas H. Airborne and terrestrial laser scanning. UK: Whittles Publishing; 2010.
[4] Yang H, Xu X, Neumann I. The benefit of 3D laser scanning technology in the generation and calibration of FEM models for health assessment of concrete structures. Sensors 2014;14:21889–904.
[5] Yang H, Xu X, Neumann I. Optimal finite element model with response surface methodology for concrete structures based on Terrestrial Laser Scanning technology. Compos Struct 2016.
[6] Jaafar HA, Meng X, Sowter A, Bryan P. New approach for monitoring historic and heritage buildings: Using terrestrial laser scanning and generalised Procrustes analysis. Struct Control Health Monit 2017:1–22.
[7] Yang H, Xu X, Xu W, Neumann I. Terrestrial laser scanning-based deformation analysis for arch and beam structures. IEEE Sens J 2017;17:4605–11.
[8] Yang H, Xu X, Neumann I. Laser scanning-based updating of a finite-element model for structural health monitoring. IEEE Sens J 2016;16:2100–4.
[9] Pesci A, Teza G, Bonali E, Casula G, Boschi E. A laser scanning-based method for fast

estimation of seismic-induced building deformations. ISPRS J Photogrammetry Remote Sens 2013;79:185–98.
[10] Cox MG. The numerical evaluation of B-splines. IMA J Appl Math 1972;10(2):134–49.
[11] Boor C. On calculating with B-splines. J Approx Theory 1972;6(1):50–62.
[12] Bureick J, Neuner H, Harmening C, Neumann I. Curve and surface approximation of 3D point clouds. Allgemeine Vermessungs-Nachrichten 2016;123:315–27.
[13] Farin GE. Curves and surfaces for CAGD. A practical guide; 2002.
[14] Piegl L, Tiller W. The NURBS book. Germany: Springer-Verlag, Berlin Heidelberg; 1997.
[15] Roncat A, Bergauer G, Pfeifer N. B-spline deconvolution for differential target cross-section determination in full-waveform laser scanning data. ISPRS J Photogrammetry Remote Sens 2011;66:418–28.
[16] Yang H, Omidalizarandi M, Xu X, Neumann I. Terrestrial laser scanning technology for deformation monitoring and surface modeling of arch structures. Compos Struct 2017;169:173–9.
[17] Zhang M, Jivkov AP. Micromechanical modelling of deformation and fracture of hydrating cement paste using X-ray computed tomography characterisation. Compos Part B 2016;88:64–72.
[18] Li HN, Li DS, Song GB. Recent applications of fiber optic sensors to health monitoring in civil engineering. Eng Struct 2004;26:1647–57.
[19] An Y, Park B, Sohn H. Complete noncontact laser ultrasonic imaging for automated crack visualization in a plate. Smart Mater Struct 2013;22(2):025022.
[20] Costanzo A, Minasi M, Casula G, Musacchio M, Buongiorno MF. Combined use of terrestrial laser scanning and IR thermography applied to a historical building. Sensors 2014;15:194–213.
[21] Nickitopoulou A, Protopsalti K, Stiros S. Monitoring dynamic and quasi-static deformations of large flexible engineering structures with GPS: accuracy, limitations and promises. Eng Struct 2006;28:1471–82.
[22] Sanchez PB, Mallorqui JJ, Duque S, Monells D. The coherent pixels technique: an advanced DInSAR technique for nonlinear deformation monitoring. Pure Appl. Geophys. 2008;165:1167–93.
[23] Chrzanowski A, Szostak-Chrzanowski A, Steeves R. Reliability and efficiency of dam deformation monitoring schemes. In: Canadian Dam Association annual conference, Canada; 2011.
[24] Bureick J, Alkhatib H, Neumann I. Robust spatial approximation of laser scanner point clouds by means of free-form curve approaches in deformation analysis. J Appl Geodesy 2016;10:27–35.
[25] Cheng X, Chen Y, Xing Z, et al. A novel online detection system for wheelset size in railway transportation. J Sens 2016:9507213.
[26] Wujanz D, Burger M, Mettenleiter M, Neitzel F. An intensity-based stochastic model for terrestrial laser scanners. ISPRS J Photogrammetry Remote Sens 2017;125:146–55.